Remote Sens. **2014**, *6*, 11627-11648; doi:10.3390/rs61111627

OPEN ACCESS

remote sensing

ISSN 2072-4292

www.mdpi.com/journal/remotesensing

Article

A Novel Methodology to Estimate Single-Tree Biophysical Parameters from 3D Digital Imagery Compared to Aerial Laser Scanner Data

Rocío Hernández-Clemente [1,*], Rafael M. Navarro-Cerrillo [1], Francisco J. Romero Ramírez [1], Alberto Hornero [2] and Pablo J. Zarco-Tejada [2]

[1] Escuela Técnica Superior de Ingenieros Agrónomos y de Montes. Dpto. de Ingeniería Forestal, Universidad de Córdoba, Campus de Rabanales, 14071 Cordoba, Spain; E-Mails: ir1nacer@uco.es (R.M.N.-C.); fj.romero@uco.es (F.J.R.R.)

[2] Instituto de Agricultura Sostenible (IAS), Consejo Superior de Investigaciones Científicas (CSIC), Alameda del Obispo s/n, E-14004 Cordoba, Spain; E-mails: alberto.hornero@csic.es (A.H.); pablo.zarco@csic.es (P.J.Z.-T.)

***** Author to whom correspondence should be addressed; E-mail: rociohc@uco.es; Tel.: +34-957-218-657; Fax: +34-957-211-010.

External Editors: Nicolas Baghdadi and Prasad S. Thenkabail

Received: 16 June 2014; in revised form: 16 November 2014 / Accepted: 17 November 2014 / Published: 21 November 2014

Abstract: Airborne laser scanner (ALS) data provide an enhanced capability to remotely map two key variables in forestry: leaf area index (LAI) and tree height (H). Nevertheless, the cost, complexity and accessibility of this technology are not yet suited for meeting the broad demands required for estimating and frequently updating forest data. Here we demonstrate the capability of alternative solutions based on the use of low-cost color infrared (CIR) cameras to estimate tree-level parameters, providing a cost-effective solution for forest inventories. ALS data were acquired with a Leica ALS60 laser scanner and digital aerial imagery (DAI) was acquired with a consumer-grade camera modified for color infrared detection and synchronized with a GPS unit. In this paper we evaluate the generation of a DAI-based canopy height model (CHM) from imagery obtained with low-cost CIR cameras using structure from motion (SfM) and spatial interpolation methods in the context of a complex canopy, as in forestry. Metrics were calculated from the DAI-based CHM and the DAI-based Normalized Difference Vegetation Index (NDVI) for the estimation of tree height and LAI, respectively. Results were compared with the models estimated from ALS

point cloud metrics. Field measurements of tree height and effective leaf area index (LAIe) were acquired from a total of 200 and 26 trees, respectively. Comparable accuracies were obtained in the tree height and LAI estimations using ALS and DAI data independently. Tree height estimated from DAI-based metrics (Percentile 90 (P90) and minimum height (MinH)) yielded a coefficient of determination (R^2) = 0.71 and a root mean square error (RMSE) = 0.71 m while models derived from ALS-based metrics (P90) yielded an R^2 = 0.80 and an RMSE = 0.55 m. The estimation of LAI from DAI-based NDVI using Percentile 99 (P99) yielded an R^2 = 0.62 and an RMSE = 0.17 m^2/m^{-2}. A comparative analysis of LAI estimation using ALS-based metrics (laser penetration index (LPI), interquartile distance (IQ), and Percentile 30 (P30)) yielded an R^2 = 0.75 and an RMSE = 0.14 m^2/m^{-2}. The results provide insight on the appropriateness of using cost-effective 3D photo-reconstruction methods for targeting single trees with irregular and heterogeneous tree crowns in complex open-canopy forests. It quantitatively demonstrates that low-cost CIR cameras can be used to estimate both single-tree height and LAI in forest inventories.

Keywords: tree height; LAI; low-cost camera; 3D image modeling; ALS data; oak forest

1. Introduction

Remote sensing of forest biophysical variables is currently a matter of growing interest for forest yield assessment, bio-energy production, and the study of the global carbon cycle. Leaf area index (LAI) and canopy height are key variables when the goal is to model ecosystem productivity by characterizing the structure and the functioning of vegetation. Leaf area index, defined as the ratio of leaf area (m^2) per ground area (m^{-2}), is one of the most important biophysical variables for modeling vegetation functioning and biomass production. Accurate and efficient LAI mapping methodologies based on remote sensing data are required to avoid having to use expensive *in situ* techniques in forest areas. Optical remote sensing of LAI relies on spectral sensitivity to changes in vegetative components in the visible and near-infrared wavelengths. Such changes have mainly been analyzed using the Normalized Difference Vegetation Index (NDVI) spectral reflectance index [1,2]. Satellite observations acquired with medium- and coarse-resolution optical sensors have been widely used to monitor seasonal and interannual variations in the amount of vegetation in forest areas [3–5]. The low spatial resolution of LAI mapping products is a limiting factor when work is conducted at a local scale, particularly in heterogeneous and sparse forests. This issue could be solved by combining medium and coarse spatial resolution satellite data [6], using high-resolution image sensors provided by commercial satellite sensors such as Ikonos, QuickBird, or RapidEye [7], or using airborne platforms [8].

In recent years, use of airborne laser scanner (ALS) data to characterize vertical structures using discrete return or full-waveform Light Detection and Ranging (LiDAR) technology has considerably increased [9–11]. The rate of transmission of laser pulses through the canopy is mathematically related to the gap fraction or the effective leaf area index (LAIe), which represents the proportion of gaps and canopy closure, respectively [11]. Several penetration ratio formulations have been applied to provide an indicator of the density of foliage in forest canopies [12]. Zhao and Popescu [13] used various types

of total numbers of penetrating hits. They obtained the highest accuracy by considering the total number of laser hits as denominators and both inside-canopy and ground hits as penetrating echoes in the numerator. Other studies [12] have demonstrated the accuracy of LAI estimations of Scots pine plots using the penetration rate derived from ALS data and fitting the relationship to a log-transformed version of the model.

Other traditional approaches to ALS data analysis have mainly focused on estimating other types of structural variables such as canopy height, tree density or basal area [14–16]. Among such variables, canopy height is an important parameter in forestry management that is used as the main input to estimate site quality, aboveground biomass stocks and spatial variation in forest stocks. The accuracy of these variables at estimating individual trees and plots essentially depends on the accuracy of tree height measurements. Use of ALS data has been proposed using two different methodologies: (1) area-based approaches [14,17–22] and (2) individual/single-tree detection approaches [23–27]. Canopy height ALS-based estimations have been widely validated by various authors at the stand level in various types of forest [17–19] and using different pulse densities [20,21]. Most of these studies have dealt with modeling approaches validated at the stand level [14,22]. Individual tree estimation is more challenging because it involves additional uncertainties, such as accurate tree position or accurate tree-level measurement inventories [23–27]. Because of this, individual tree estimation is more expensive and requires greater pulse density, field measurement and computational effort [10].

The recent fast growth in digital photogrammetric technology has opened a new option for remote sensing applications which is leading to significant cost reductions. Apart from ALS data, digital aerial imagery (DAI) can also be used to creating a forest canopy surface model [28]. 3D digital photogrammetry is rapidly evolving and cost-efficient solutions using consumer-grade digital cameras are currently being proposed as an alternative to LiDAR technology [29]. This offers the possibility of using consumer-grade digital cameras of around (<5000 €) compared with ALS sensors (>100 k€). In addition, the recent progress in low-cost integrated GPS systems and inertial sensor devices for remote sensing applications [30] opens new possibilities in forestry. Improvements in these systems and readily available photogrammetric software packages for inexperienced users have been critical to validate such systems and devices. In fact, several studies have focused on validating these products and comparing them to ALS data [31,32]. Several approaches have been proposed for combining stereo-photogrammetric measurements with LiDAR data for the retrieval of canopy height. For example, St-Onge *et al.* [33] measured tree height manually in a coupled Ikonos-LiDAR model and obtained a mean error of 2.58 m. The main disadvantage of this type of approaches is the need for co-registration of the photogrammetric digital surface model (DSM) to a LiDAR digital terrain model (DTM). The most accurate alternative, which provided sub-pixel accuracy in horizontal coordinates given the same limitations (e.g., the same on-flight Global Navigation Satellite System errors) was proposed by Valbuena (2014) [34]. Another disadvantage is the dependence on ALS data to create a canopy height model (CHM) from a photogrammetric DSM. A recent study [35] has demonstrated that digital images can be used successfully to estimate tree height using a CHM obtained by calculating the difference between the minimum DSM value (ground height) and the maximum elevation (treetop). Specifically, a root mean square error (RMSE) of 0.34 m and a relative root mean square error (RRMSE) of 11.5% were obtained in young regular orchard plantations lower than 4 m cultivated on a flat surface. Unfortunately, this approach should not be used with uneven terrain, as differences in the reference value of ground height

around the canopy would affect the accuracy of the estimation of total tree height. However, studies on the application of this solution to forest inventories are still very limited in the literature, largely because of the many variables that influence the accuracy of tree height estimation based on DAI and of inaccuracies in field measurements and GPS locations [28]. These problems are particularly severe in forest canopies in areas with hilly terrain and a high degree of crown overlapping. None of the above-mentioned studies have analyzed the retrieval of forest variables, such as LAI or tree height, from individual trees using DAI data alone in forest areas. Our intention was to fill this gap and assess the capability of using an alternative and low-cost technology to obtain tree height and LAI estimates as compared to ALS-based methods. The primary objective of this study was to develop a method to create a CHM of individual trees based on 3D photo-reconstruction methods using spatial interpolation techniques to improve tree height estimations. Additionally, we proposed to combine a DAI-based CHM with radiometric information obtained from color infrared (CIR) aerial images to estimate LAI from DAI data. We also performed multiple regression analyses to predict tree height and LAI based on a selection of optimal metrics derived from DAI and ALS data, respectively.

2. Materials and Methods

2.1. Study Site Field Data Measurements

The study area was located in Huelva province, in southwestern Spain (Lat 37°36′30.89″N, Lon 7°20′27.97″W). This area is dominated by mature trees of the evergreen species *Quercus ilex* subsp. Bellota, with an average density of 40 trees per ha (Table 1). The topography was slightly hilly, with altitudes ranging between 171 to 234 m above sea level and acidic and poor soils. Trees had shown symptoms of decline (*i.e.*, defoliation and branch dieback) since the 1990s and high mortality rates since the 2000s [36]. This factor was critical to sample trees with a similar structure and a different range of LAI values.

Table 1. Tree statistics of the samples measured (average, maximum, minimum values and standard deviation (SD)).

Forest variable	Average	Max.	Min.	SD
Trunk diameter (cm)	39.01	79.7	11.00	12.19
Trunk height (m)	1.78	3.50	0.00	0.49
Tree height (m)	6.61	10.50	2.00	1.36
Crown diameter (m)	9.10	16.00	4.05	2.57
LAI	1.00	1.69	0.49	0.34
Density (trees/ha)	47.74			

In February 2013, we visited the oak forest several times to develop a forest inventory and to collect LAI measurements. All of the trees in an area of 4.26 ha (*i.e.*, a total of 200 trees) were located using a GPS device (GPSMAP 60CSx, Garmin International, Inc.) with a spatial accuracy below 5 m. From those trees, we recorded the following measurements: diameter at 1.3 m height and total tree height. Additional measurements of LAI values were taken from a subsample of 26 trees of this data set. Total tree height was estimated using an ultrasonic hypsometer (Vertex IV; Haglöf Sweden AB, Långsele,

Sweden) with a height resolution of 0.1 m, using the average of a total of three different measurements collected by two different technicians. LAI was measured using the LAI-2000 Plant Canopy Analyzer (LI-COR, Inc., Lincoln, NE, 1992) and positioning the optical sensor in four different orientations under the canopy, at a 1 m distance from the ground and using a cup that covered 90° of the field of view affected by the trunk. Measurements included a reference reading above the canopy and below-canopy readings. All measurements were taken before sunrise, after sunset, or under a uniformly overcast sky.

2.2. DAI and ALS Data Acquisition

Airborne campaigns were conducted in 2013 with two different sensors and acquisition settings. The aerial imagery was obtained by the Laboratory for Research Methods in Quantitative Remote Sensing (QuantaLab, Institute for sustainable agriculture (IAS), Spanish National Research Council (CSIC), Spain) in February 2013. Image acquisition was performed using a consumer-grade camera modified in the laboratory for color infrared detection by removing the internal infrared filter. The camera was a Panasonic Lumix DMC-GF1 (Panasonic Corporation, Osaka, Japan) with a 4000 × 3000 pixel detector that captured images at f/2.8 and 1/2000 s with an angular field of view (FOV) of 47.6° × 36.3° and provided ~12 cm per pixel resolution at an altitude of 500 m above ground level. Radiometric calibration was performed after applying channel decomposition, which consists of setting the infrared camera to a custom white balance and using an 850 nm long pass filter through a white card. These settings produce channel gains in the infrared. Finally, in order to extract the green (G) and red (R) gains, blue (B) was subtracted from G and R as all RGB channels receive the same light from the infrared (IR). The imagery was synchronized using the GPS position and triggering time recorded for each image. In this study, only absolute GPS coordinates were used to generate ortho-mosaics and DSMs; no relative data from inertial units were used as input.

The airborne image acquisition flight plan was specifically designed to ensure the collection of very high resolution (VHR) imagery and large across- and along-track overlapping over the field. The aim was to ensure that the photo-reconstruction method used later to derive the DSM from the VHR imagery would be able to retrieve a large number of image targets, allowing successful reconstruction. The area was therefore flown over using a grid of parallel and perpendicular flight lines (Figure 1) to ensure that each ground object was imaged in the along- and across-track directions of the airborne platform, maximizing overlap. A cloud of images comprising both sets of flight lines covered the entire area homogeneously at a rate of 2 s between consecutive images, considering variations in the ground speed of the flight due to changeable wind conditions (Figure 1). At an average 120 km/h ground speed, an FOV = 47.6° × 36.3° and an altitude of 500 m, the resulting average overlapping obtained during the flights was extremely large and was estimated at 80–90% in most cases (Figure 1).

ALS data were acquired by Heligrafics (Alicante, Spain) in March 2013 with a Leica ALS50-II laser scanner (Leica Geosystems AG, Heerbrugg, Switzerland) with a laser repetition rate of 178.6 kHz, a scan frequency of 100 Hz and an FOV of 13 degrees. The field was scanned by plane from a flight altitude of 1300 m above ground. ALS data were acquired with a point density of 12 points/m^2. They were geo-referenced in the European Terrestrial Reference System 1989 (ETRS89) coordinate system. Planimetric coordinates (x and y) and ellipsoidal height values were computed for all echoes.

Figure 1. (**a**) Digital aerial image acquisition planning: spatial distribution of images acquired over the area. (**b**) Flight log showing the grid from east to west.

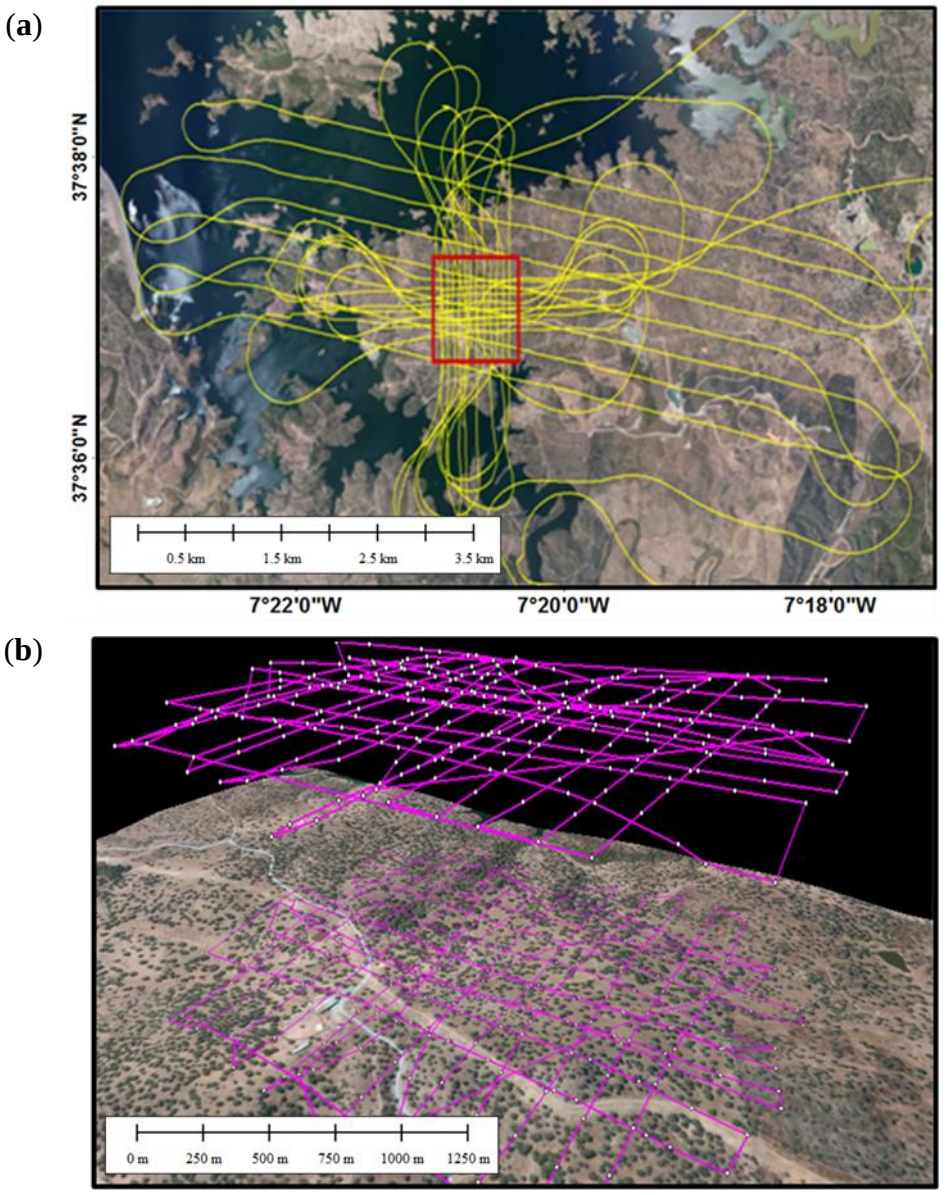

2.3. ALS- and DAI-Based Metrics

Feature extraction was performed separately for ALS and DAI data at crown level (Figures 2 and 3). In both cases, crowns were delineated following the multiresolution segmentation approach [37] (Figure 4), using the ALS-based CHM for ALS data analysis and the NDVI for DAI data analysis. The parameters used for implementing the multiresolution segmentation algorithm were determined empirically by visual analysis. In the first case, the segmentation parameters were a scale of 6, shape of 0.2 and compactness of 0.8 using an ALS-based CHM with a resolution of 1 m. In the latter case, the segmentation parameters were a scale of 80, shape of 0.8 and compactness 0.4, using an NDVI with a resolution of 0.12 cm. Given the fact that there is no validated delineation method available yet for the combined comparison of the accuracy of ALS and DAI in retrieving *in situ* LAI and tree height, the results were cross-validated using manual delineation. Figure 4b,c show an overview of the crown delineation

obtained in each case. The ALS-based CHM for ALS data was estimated following the methodology described in [20]. Figure 2 shows an example of the CHM estimated from ALS and DAI data. Additionally, Figure 3 shows a side view of a profile of ALS data overlaid with DAI. The ortho-rectified color infrared aerial images were also used to calculate the Normalized Difference Vegetation Index (NDVI) using the near-infrared (NIR) and the red (R) bands as (NIRCIR − RCIR)/(NIRCIR + RCIR).

Figure 2. (**a**) Example of the ALS-based canopy height model. (**b**) Digital aerial imagery (DAI)-based canopy height model. (**c**) ALS cloud points overlaid on the DAI-based canopy height model.

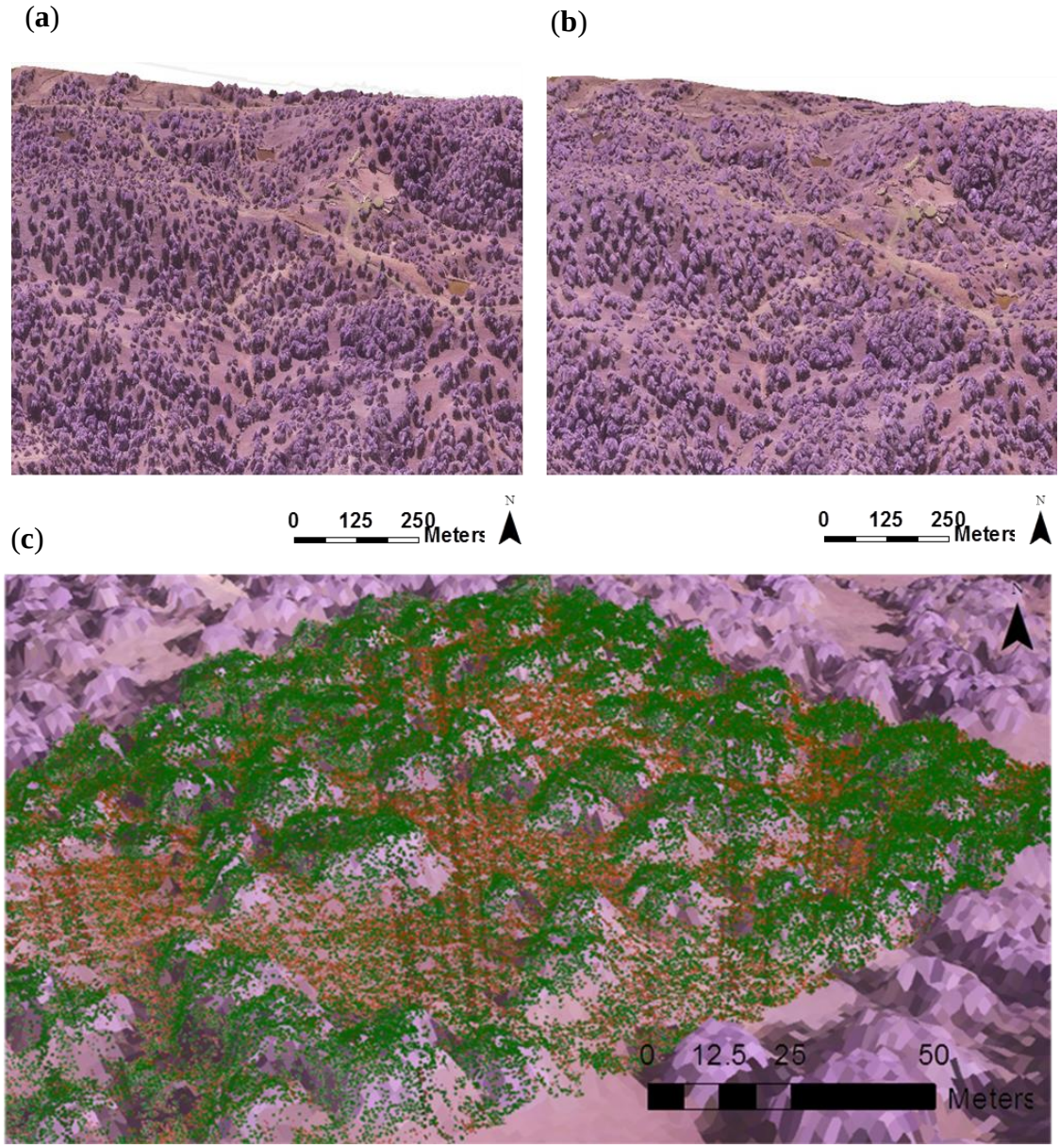

Figure 3. Example of a side view of a profile of an ALS-based and a DAI-based canopy height model overlaid with a 3D photogrammetric digital surface model reconstruction. Profile width = 1 m, length = 105 m.

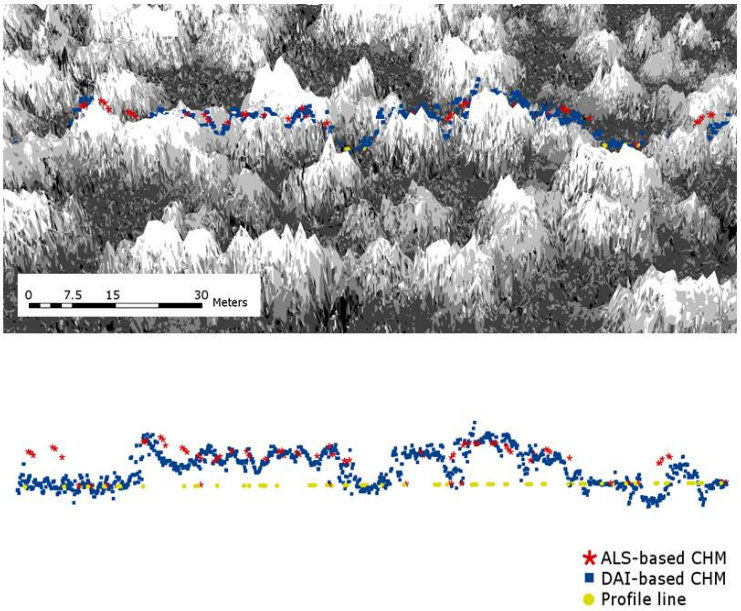

Figure 4. (**a**) Soil buffering around overlapping and non-overlapping crowns as a reference for the spatial interpolation of ground points under the canopy. (**b**) Object-based delineation of crown trees based on DAI data. (**c**) Object-based delineation of crown trees based on ALS data. In both cases, manual delineation (dotted orange line) was used as the background.

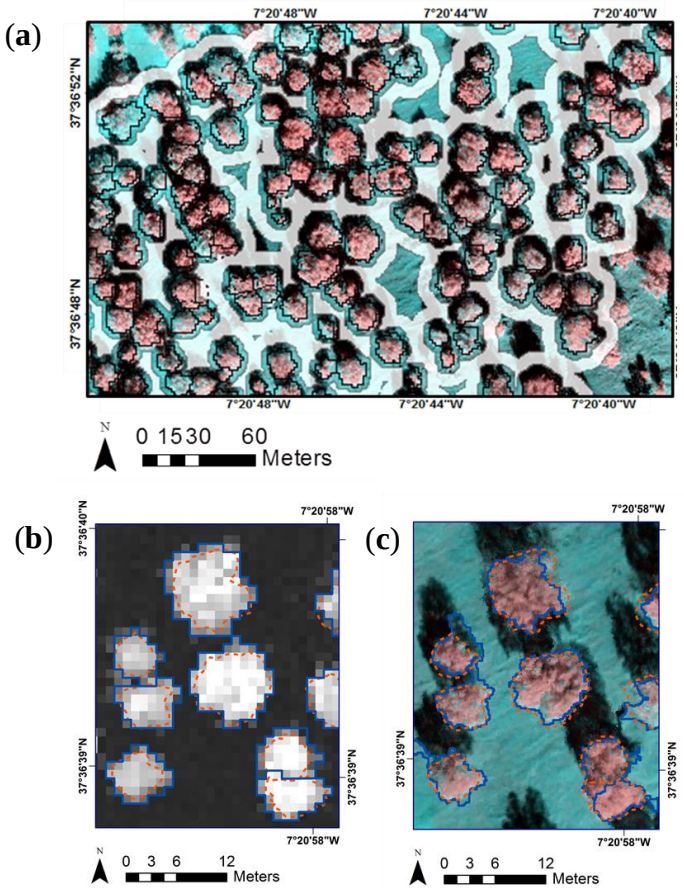

After crown delineation processing, data were extracted from ALS and DAI data. Tree height was modeled separately from metrics derived from the ALS raw points and from the DAI-based CHM. LAI was also modeled separately, using ALS-based metrics when ALS data were analyzed and a combination of the DAI-based NDVI and the DAI-based CHM when DAI data were analyzed.

The ALS raw point cloud data were processed and filtered using TerraScan software (Terrasolid, Finland). After removing erroneous points, discrete returns were classified using the progressive triangular irregular network densification algorithm [38]. Ground points were classified using the following geometric conditions: maximum terrain slope of 88°, iteration angle of 7° and iteration distance of 0.50 m. Any points that remained unclassified were considered as the vegetation class. Next, metrics were extracted from the ALS point cloud data using the Cloud Metrics tool from the FUSION LiDAR Toolkit [39].

The DAI-based CHM was calculated as the relative difference between the DSM and ground height. A high-resolution photogrammetric DSM was generated with Pix4D software (Ecublens, Switzerland) using a total of 287 images from the flights conducted over the field (Figure 2) and applying the structure from motion (SfM) method. The methodology used, described in a paper written by Zarco-Tejada *et al.* [35], included automatic aerial triangulation, bundle block adjustment, and DSM and ortho-mosaic creation. Table 2 provides a detailed description of the parameters used to generate the DAI-based CHM. Given that compact cameras generally used in aerial platforms are extremely sensitive to temperature differences, vibrations, and shocks, one of the processing steps was camera auto-calibration. This involved using information from each pixel of the images to estimate the optimal camera and lens calibration for each flight. The imagery and synchronized GPS position for each single image were used as the input. The point cloud densification was set to high, and the grid sampling distance in the digital elevation model point cloud was set to 1 m. The true ortho-mosaic obtained had 5000 × 5000 pixel tiles with a blending factor of 0.5 and ~12 cm per pixel resolution, covering a total of 145 ha. The camera parameters were optimized internally during the first step conducted.

Table 2. Parameters used to generate the DAI-based canopy height model.

Image acquisition Parameters		**Image Processing**	
Images acquired	552	Total key point observations	104,950
Images used	287	Total 3D points	39,636
Mosaic area (ha)	145.19	Mean reprojection error (pixels)	0.7525
* GSD (cm)	12.74		

* GSD, ground sampling distance.

Ground height under the crowns was calculated using the Kriging technique by taking a weighted linear average of available sample data points in close proximity to the area of interest. The key aspect of this process is that weights are determined from the spatial dependence represented by the semivariogram [40]. Bare soils points were obtained within a 2 m buffer around the crown shape (Figure 3). The accuracy of the interpolated data under the canopy can be affected by two variables: the specific variations in ground height under the canopy or in the slope of the ground; or the percentage of data around the crown used in the interpolation, a variable that is limited by the percentage of overlapping and non-overlapping crowns. Such a percentage was estimated from the buffer area defined around the

tree crown delineation. The sensitivity of the resulting DAI-based CHM to the terrain slope and the percentage of crown overlapping were assessed by exploring the relationships between those variables and the difference between predicted and observed samples. Both variables were calculated with geoprocessing tools implemented in ArcGIS 10.1.

Metrics separately calculated from ALS and DAI data were used to establish the regression relationship with ground reference tree height and LAIe estimates. Metrics derived from each data set (*i.e.*, DAI and ALS data) were analyzed and compared to one another in order to assess the potential of each technology (Table 3). Tree height models were based on metrics calculated from the DAI-based raster CHM and from the ALS-based raw point clouds. LAI models were based on metrics calculated from the DAI NDVI when DAI data were used and from the normalized laser penetration index (LPI) estimated from the raw point cloud when ALS data were used. The LPI was calculated from ALS-based echo returns as:

$$LPI = (\sum Nbfr)/(\sum Na) \quad (1)$$

where N_{bfr} was the total number of first below-canopy returns and N_a was the total number of returns (from high vegetation and ground points, respectively). Only first echoes were used, as the last and intermediate echoes provide very little information [9].

Table 3. Metrics derived from DAI and ALS data.

Label	Description
Min	Minimum
Max	Maximum
Mean	Mean
SD	Standard deviation
Var	Variance
CV	Coefficient of variation
IQ	Interquartile distance
Skew	Skewness
Kur	Kurtosis
AAD	Average absolute deviation
L1, L2, L3, L4	L-moments (L1, L2, L3, L4)
L CV	L-moment coefficient of variation
L skew	L-moment skewness
L kur	L-moment kurtosis
P01…P99	Percentiles

2.4. Statistical Model Analysis

Both simple linear and multiple regression models were analyzed using DAI- and ALS-based metrics as predictors of field data measurements. The latter models were fitted applying the optimization of linear models based on the least squares method also known as 'REG' procedure [41] implemented with SAS/STAT® software (SAS Institute Inc., Cary, NC, USA, 2004). For each variable, the REG procedure indicates the proportion of the variance of the estimate accounted for by each principal component. To account for multicollinearity in explanatory variables, we performed a variable selection using the high

condition index contributes strongly (*i.e.*, variance proportion greater than about 0.5) to the variance of two or more variables. The variables included in the model were selected using Mallows' process capability index (Cp) method in the REG procedure, which performs all possible subset regressions and lists the models in ascending order of Cp. Multicollinearity among the explanatory variables was verified with the condition index, in line with the findings of Belsley [42]. Consequently, all of the variables selected and included in the models developed to retrieve height and LAI variables had a condition index lower than 30 and a *p*-value less than 5%.

The model was validated based on the root mean square error (RMSE) (Equation 2) and relative RMSE (RRMSE) (Equation (3)) along with the regression fit and the squared correlation coefficient between predicted and observed tree height and LAI; such values were assessed for each data set derived from ALS and DAI data.

$$RMSE = \sqrt{\sum_{i=1}^{n} \frac{(O_i - P_i)^2}{n}} \quad (2)$$

$$RRMSE = \sqrt{\sum_{i=1}^{n} \frac{(O_i - P_i)^2}{n}} . \frac{1}{\overline{O}} \quad (3)$$

In Equations (2) and (3), O_i is the observed value, Pi the predicted value, n the total amount of measurements and $\overline{\boldsymbol{O}}$ the average of the observations.

3. Results

3.1. Canopy Height Estimation from ALS and DAI Data

Based on the analysis described above, simple linear and multiple regression models were applied to evaluate the accuracy of DAI- and ALS-based metrics separately in retrieving *in situ* tree height. As regards the accuracy analysis of the estimated regression function with field-derived tree height measurements and DAI- and ALS-based metrics, the coefficient of determination (R^2) is shown in Figure 5. Overall, simple linear regression model results showed that the performance of most metrics extracted from ALS point data was better than that of metrics extracted from photogrammetric DAI in estimating canopy height. In both cases, significant results ($p < 0.05$) were obtained with percentiles ranging from P30 to P99. The highest accuracy was obtained using P90 (Figure 6), which yielded a coefficient of determination of $R^2 = 0.80$ for ALS-based metrics and $R^2 = 0.67$ for DAI-based metrics. The maximum, mean, median, variance, and average absolute deviation (AAD) yielded significant values with both types of metrics, with a coefficient of determination of $R^2 = 0.54–0.74$ for ALS-derived metrics and $R^2 = 0.5–0.62$ for DAI-derived metrics (Figure 5). However, none of these metrics yielded better accuracy than that of percentiles ranging from P75 to P99.

Figure 5. Coefficient of determination (R^2) derived from the relationship between tree height and maximum, mean, variance, average absolute deviation (AAD), L-moments (L1, L2), and percentile values (5th, 10th, 20th, 25th, ..., 95th percentiles) derived from the ALS-based and the DAI-based data.

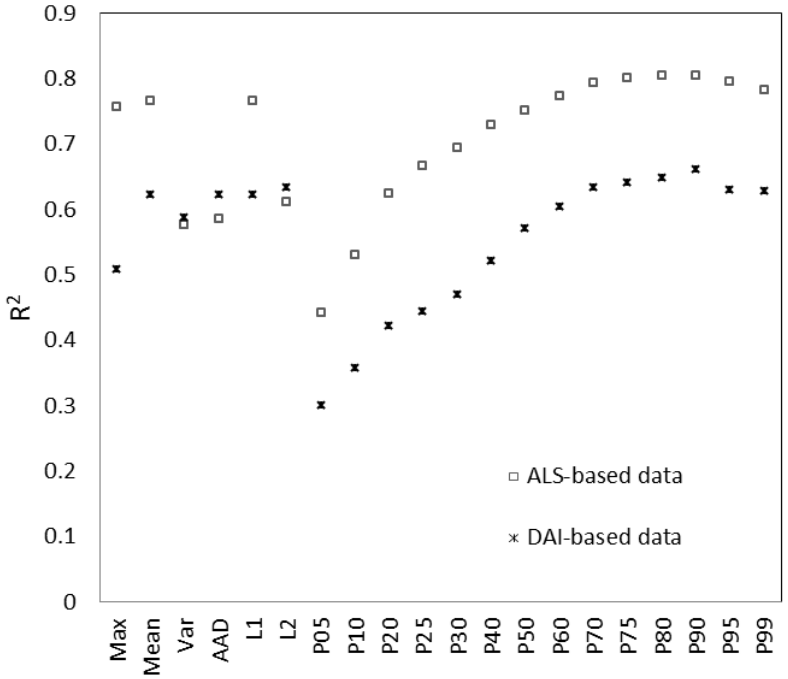

Figure 6. (**a**) Relationship between observed height and ALS-based data using the 90th percentile. (**b**) Relationship between observed height and the DAI-based data using the 90th percentile. Regression function (solid lines) and 1:1 correspondence (dashed lines). CHM, canopy height model.

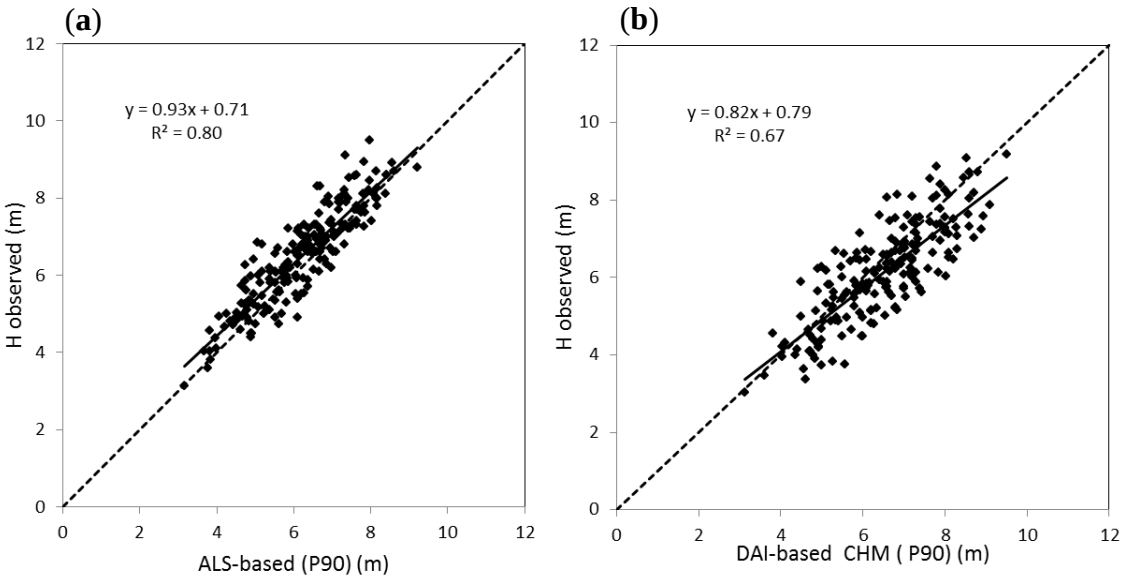

In order to analyze the factors that affected the above-mentioned relationships, we explored the effects produced by the percentage of crown overlapping and slope. Figure 7 shows the results of the difference between predicted and observed tree height as $(H - Ho)^2$ using DAI and ALS data. According to these

results, model performance was not significantly affected (*p*-value > 0.05) by the percentage of slope or crown overlapping. This result is relevant to demonstrate that the proposed method was not affected by the structure of the vegetation canopy or ground unevenness.

Figure 7. (**a**) Difference between predicted and observed height $(H - Ho)^2$ in relation to the percentage of crown overlapping using the DAI-based canopy height model and ALS data. (**b**) Difference between predicted and observed height $(H - Ho)^2$ in relation to the slope using the DAI-based canopy height model and ALS data.

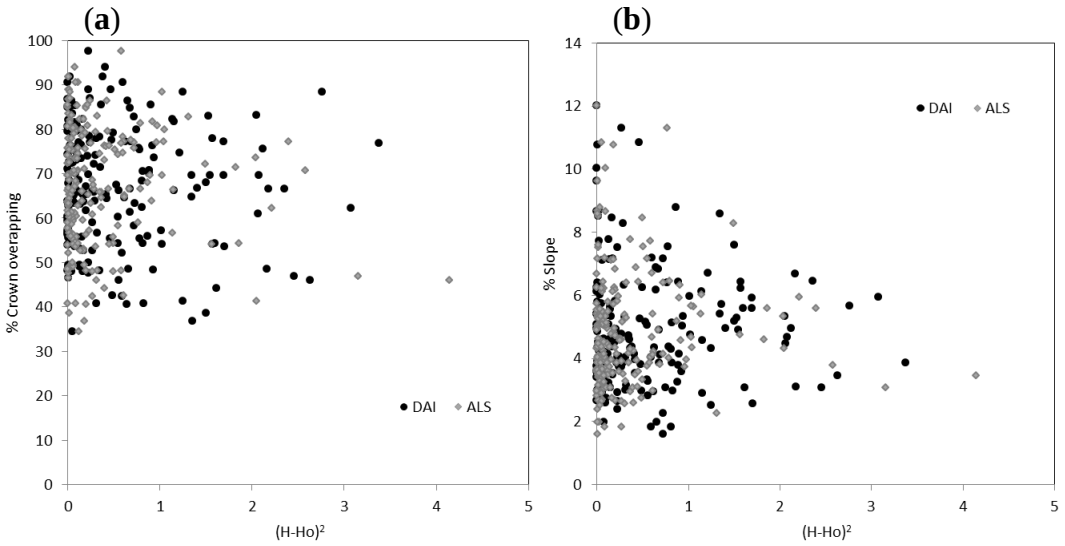

The last stage of this research was to obtain the results of the best multiple regression fitting models for the retrieval of tree height. Results of model fitting and selecting ALS- and DAI-based metrics for the estimation of tree height are summarized in Table 4. We obtained coefficients of determination of $R^2 = 0.8$ using ALS-based metrics and $R^2 = 0.71$ using DAI-based metrics, yielding an RMSE = 0.51 m (RRMSE = 7.9%) and an RMSE = 0.71 m (RRMSE = 10.90%), respectively. The multicollinearity analysis based on the condition index applied during the subset selection and fitting process limited the metrics included in the final models. As a result, models were based on one single variable (P90) in ALS data sets and on two variables (P90, Hmin) in DAI datasets. Nevertheless, few differences were found regarding the strength of correlation using the final models fitted from both data sets, as shown in Figure 8. Cross-validation results obtained using manual delineation were similar, with an RMSE = 0.51 m for model predictions based on ALS data and an RMSE=0.71 m for model predictions based on DAI data.

Table 4. Results of the best models obtained for the estimation of tree height from ALS- and DAI-based metrics.

	Variable	**Parameter**	**Standard Error**	***t*-Value**	***p* > |t|**	**R^2**
Method	Intercept	73.69	33.13	2.22	<0.01	
DAI-based tree height	P90	0.79	0.04	19.31	<0.001	0.71
	Hmin	−35.97	16.53	−2.18	<0.01	
Method	Intercept	0.71	0.20	3.43	<0.001	0.80
ALS-based tree height	P90	0.93	0.03	28.43	<0.001	

Figure 8. Field-observed *versus* ALS-predicted tree height. (**a**) Field-observed tree height *versus* (**b**) DAI-predicted tree height. The graphs show the regression function (solid lines) and 1:1 correspondence (dashed lines).

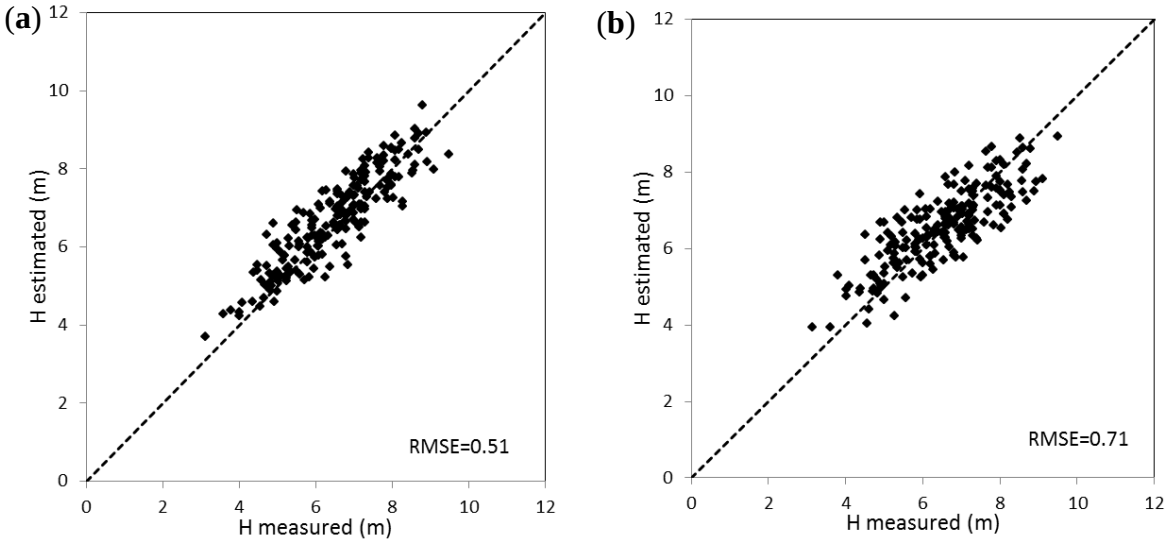

3.2. LAI Estimation from the ALS Data and DAI-Based Canopy Height Model

The accuracy analysis of the estimation of LAI at the crown level was first evaluated based on simple linear regression models obtained from ALS- and DAI-derived metrics. As regards ALS-derived metrics, significant relationships were found between the LPI and *in situ* LAIe, with a coefficient of determination of R^2 = 0.64 (Figure 9). As regards DAI-derived metrics, as shown in Figure 10, significant relationships ($p < 0.05$) were also obtained for LAIe using percentiles ranging from P30 to P99 derived from DAI NDVI data. In this range, the best relationships were obtained using the higher percentiles (P75 to P99), which improved the results obtained with the maximum, mean or median metrics.

A multiple variable model analysis was subsequently applied; results of the best models are shown in Table 5. Subset variable selection was conducted considering metrics derived from ALS and DAI data separately. The subset selection made to agree with Mallows' Cp criterion yielded a small number of variables to consider in both cases. For DAI-based estimations, the model included P99 (DAI NDVI), and the rest of the variables were rejected based on their significance and/or collinearity. For ALS-based estimations, the model included three variables (LPI, interquartile distance IQ and P30). According to the validation assessment performed with field-observed LAIe, model predictions based on ALS data yielded a coefficient of determination of R^2 = 0.75, an RMSE = 0.14 m^2/m^2 and an RRMSE = 15.71% compared to an R^2 = 0.63, an RMSE = 0.17 m^2/m^2, and an RRMSE = 17.67% using DAI data (Figure 11). Cross-validation results obtained using manual delineation yielded similar results with an RMSE = 0.13 m^2/m^2 for model predictions based on ALS data and an RMSE = 0.17 m^2/m^2 for model predictions based on DAI data.

Figure 9. Relationship between observed effective (LAIe) and the laser penetration index (LPI) (1) obtained from ALS data.

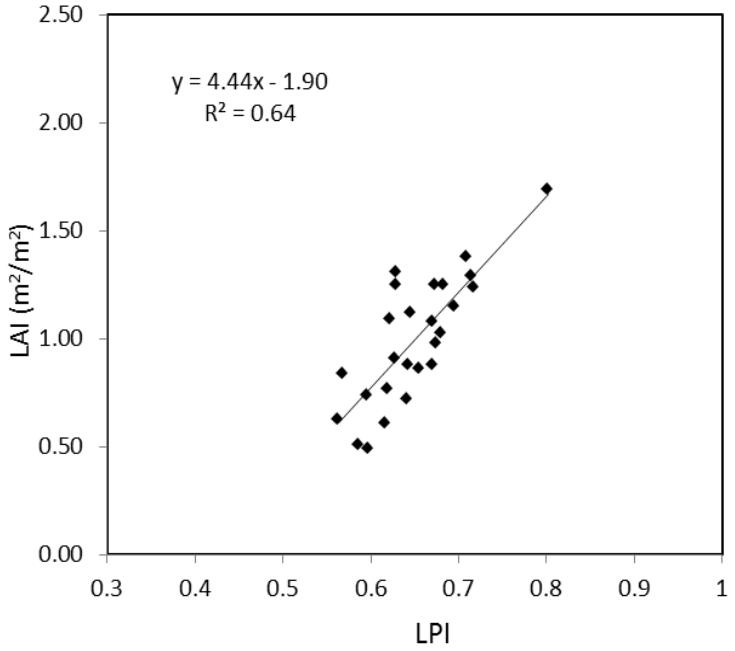

Figure 10. Coefficient of determination (R^2) derived from the relationship between LAIe and maximum, mean and percentile values (5th, 10th, 20th, 25th, ..., 95th percentiles) derived from the DAI-derived Normalized Difference Vegetation Index (NDVI).

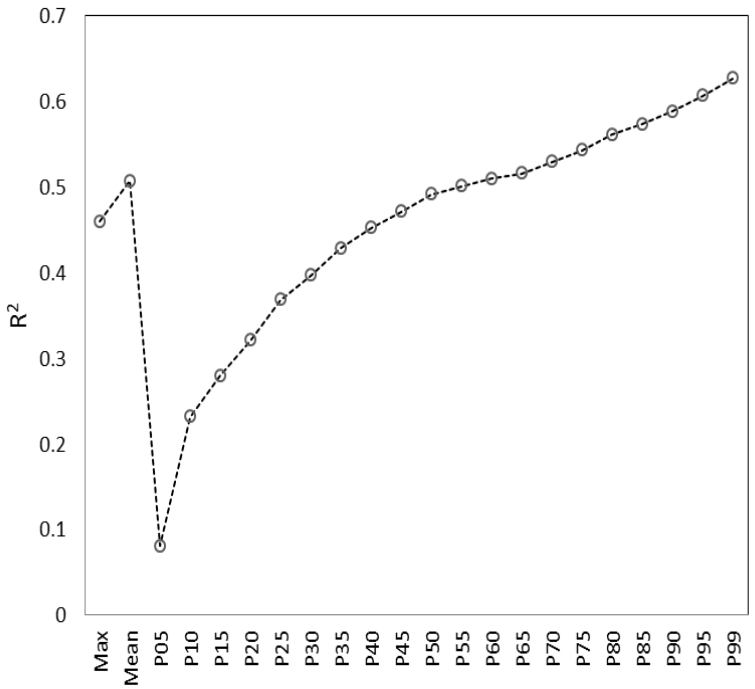

Table 5. Results of the best models obtained for the estimation of LAI from ALS- and DAI-based metrics

	Variable	Parameter	Standard Error	*t*-Value	$p > \|t\|$	R^2
Method						
DAI-based LAIe	Intercept	−1.04	0.32	−3.22	<0.001	0.62
	P_{99} DAI NDVI	9.38	1.47	6.34	<0.001	
Method						
ALS-based LAIe	Intercept	−2.65	0.77	11.63	<0.001	0.75
	LPI	4.78	1.01	22.38	<0.001	
	IQ	0.07	0.03	4.78	<0.01	
	P30	0.06	0.02	8.06	<0.01	

Figure 11. (**a**) Field-observed effective leaf area index (LAIe) *versus* ALS predicted LAI (**b**) Field-observed effective leaf area index (LAIe) *versus* DAI predicted LAI. Graphs show the regression function (solid lines) and 1:1 correspondence (dashed lines).

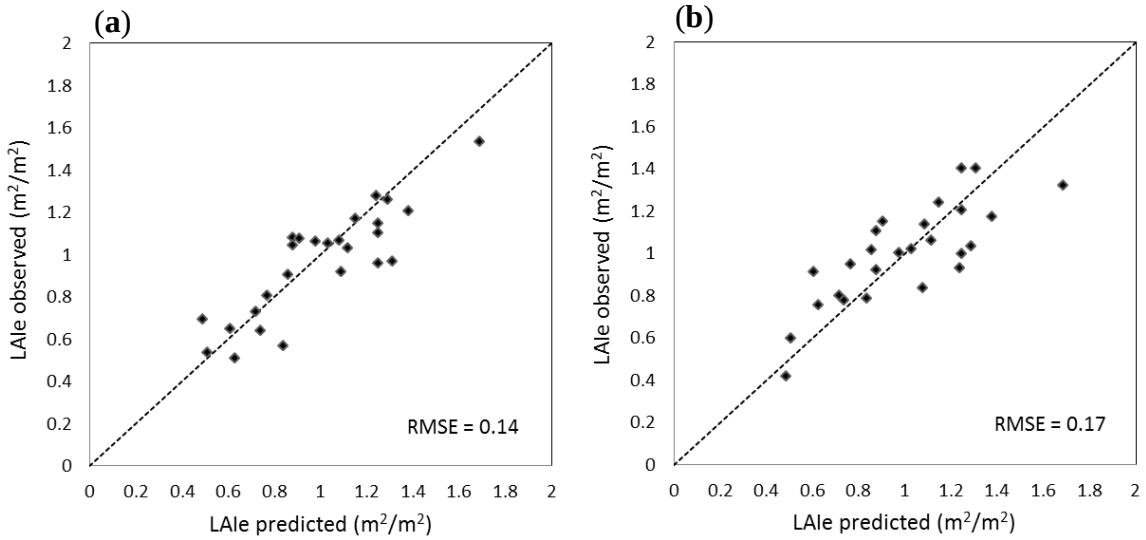

4. Discussion

Although ALS technology is an effective tool in forest inventory development, it still requires expensive laser scanning systems and complex processing methods that make it difficult to update inventory data regularly. This study shows the results of estimating two key parameters (*i.e.*, LAI and tree height) using 3D reconstruction from airborne imagery, an alternative low-cost technology.

The main challenge in the direct estimation of tree height from DAI data is to accurately calculate the CHM since ground height data under the canopy is missing. Most of the progress made using digital imagery approaches relies on the retrieval of ground height data from LiDAR elevation models [33]. Because the main aim of this research was the validation of DAI-based CHM independently from ALS data, in this study we propose a new methodology based on the spatial interpolation of ground height under the canopy. Previous studies have tested other methodologies without obtaining satisfactory results. For instance, Järnstedt *et al.* [28] calculated the difference between photogrammetric DSMs and an ALS-based DTM, yielding RMSE values of 3.48 m and a relative root mean square error (RRMSE)

of 18.61% for the estimation of dominant heights. Apart from the uncertainty of results, the main disadvantage of this method is that it involves the use of ALS data. An alternative methodology was proposed by Zarco-Tejada *et al.* [35] using local reference values of ground height and DSM local maxima from a square 3 × 3 m kernel. This methodology may not be adequate in hilly terrain and when targeting overlapping forest canopies, as the uncertainty of the reference ground height around the crowns increases. By contrast, our proposed method based on spatial interpolation greatly contributed to improving the accuracy of the estimation of structural variables over forest canopies. Moreover, according to our results, the reliability of the models was not significantly influenced by the percentage of crown overlapping or the slope of the terrain. These results suggest that, considering similar land surfaces and canopy structures (*i.e.*, average values of 4.81% ± 1.83 of slope and 67.07% ± 13.36 of overlapping), the methodology proposed seems to contribute to improving the accuracy of the estimation of forest structural variables. Yet, the complexity of the vegetation structure of this study was relatively low, compared to other types of canopies with higher tree density and species composition. Therefore, future studies should be conducted with different levels of crown overlapping, canopy density, and slope. At present, the progress made with this study contributes to the application of low-cost approaches based on the use of consumer cameras to meet the critical requirements in 3D data for the estimation of tree height and LAI in open-canopy forests.

Another important issue that requires attention is the delineation method applied to compare the accuracy obtained using ALS data *versus* DAI data. Although the multiresolution segmentation method was cross-validated with manual delineation in this study, the robustness of this approach should be further validated in other types of canopies with a different structure and heterogeneity.

To the best of our knowledge, very few studies have focused on estimating forest structural parameters based on photogrammetric CHMs [15,17,29,43,44], and even fewer studies have jointly estimated LAI and tree height at the crown level. Most studies have assessed variables such as height, diameter, and stem volume combining ALS data and aerial photograph features at the stand level [45] and at the tree level [46]. However, the results of this study demonstrate that the use of DAI data for the retrieval of tree height can yield reasonable RMSE values (RMSE = 0.71 m) that are comparable to those obtained from ALS data (RMSE = 0.55 m) using either data set. In addition, the main source of error when estimating structural variables from individual oak trees may be related to the heterogeneity and flattened geometry of crowns. These factors increase inaccuracies in the measurements of total tree height, including errors derived from field data measurements and errors derived from ALS- or DAI-based metric estimations. Yet, it should be noted that the accuracy of DAI-based models showed the same pattern as that of ALS-based models, with the highest coefficients of determination (R^2 = 0.80 and R^2 = 0.67, respectively) obtained with the same metric (P90).

Results of LAIe estimation using ALS and DAI data yielded similar results (R^2 = 0.75 and R^2 = 0.62, respectively) and a root mean square error of about 0.1 m^2/m^2 in both cases. The most important finding of this study was that LAIe can be estimated with reasonable accuracy using DAI radiometric data alone (RMSE = 0.17). These results suggest that NDVI metrics derived from DAI obtained with a consumer-grade camera are a useful indicator of LAIe in the type of forest canopy explored. This opens up new possibilities for the retrieval of LAI in forest ecosystems using more affordable and less sophisticated technology than ALS technology. Yet, results showed that LAI models derived from ALS LPI, IQ and P30 metrics were the most accurate. It is interesting to note the small contribution of the IQ

and P30 to the model obtained from ALS data, which may be related to the dispersion of backscattered pulses relative to the total height of the canopy. This is clearly related to the relative amount of biomass within the canopy and, therefore, to LAI values. In addition, future studies could also focus on the improvement of LAI retrieval using both types of technologies (*i.e.*, DAI and ALS). Following this approach, the combined use of NDVI from QuickBird satellite images (with a spatial resolution of 2.4 m) and ALS data metrics was previously tested by Zhao and Popescu [13], who did not show any significant improvement compared to the use of ALS data alone. However, no quantitative validations of the use of DAI NDVI and DAI CHM-based metrics to estimate LAIe have been reported so far.

The advantage of the modeling approach proposed in this study is the simultaneous estimation of LAIe and tree height using low-cost commercial CIR cameras. Data fusion of DAI NDVI and ALS-based metrics might improve the accuracy of estimations of forest structure parameters. In this case, the use of photogrammetric point clouds (PPCs) generated by image matching may contribute to improve the method for data fusion, being a critical factor for individual tree crown analysis [34].

These results are promising because precise and updated mapping of LAI and canopy height is a key input to validate dynamic forest models such as Physiological Principles Predicting Growth model (3PG) [47], the Carbon budget model of the Canadian Forest Sector (CbM-CFS3) [48], or the model of forest growth and carbon dynamics (TRIPLEX) [49]. In addition, these results open new avenues for the development of low-cost operational solutions in forest inventory development. The possibility of using conventional CIR cameras for this purpose also makes it possible to use such sensors on unmanned aerial vehicle (UAV) platforms [35].

5. Conclusions

In the present study, we propose a new approach to generate a canopy height model (CHM) from very high resolution digital aerial imagery (DAI) acquired with low-cost commercial color infrared (CIR) cameras using the structure from motion (SfM) method as an alternative to using more sophisticated technologies, such as airborne laser scanners (ALS), in the context of complex forest canopies. Both single-tree height and effective leaf area index (LAIe) at the crown level were estimated from DAI and ALS data and compared to field data. Robust models were developed for both variables with a set of metrics derived from ALS and DAI data independently. When estimating tree height, the reliability obtained with ALS-based Percentile 90 (P90) was slightly higher than that obtained with DAI-based metrics (P90 and minimum height (Hmin)), with a relative root mean square error (RRMSE) difference of 3% (yielding an RMSE = 0.51 m and an RMSE = 0.71 m, respectively). These results represent progress in the validation of 3D photogrammetric models applied to forest inventory development. In the case of LAI estimation, the reliability obtained with ALS-based metrics (laser penetration index (LPI), interquartile distance (IQ), Percentile 30 (P30)) was slightly higher than that obtained with DAI-derived Normalized Difference Vegetation Index (NDVI) metrics (DAI NDVI P99), with an RRMSE difference of 1.96% (RMSE = 0.14 m^2/m^2 and RMSE = 0.17 m^2/m^2, respectively). Our results demonstrated that the estimated error obtained for both the tree height and LAI parameters using low-cost airborne digital imagery was not significantly affected by the slope or the percentage of crown overlapping typically observed in an oak forest canopy. This notwithstanding, the successful retrieval of single-tree and forest-stand biophysical variables using low-cost digital airborne imagery in other canopy

types and terrain characteristics should be further analyzed and validated to assess issues related to canopy heterogeneity, crown dimensions and tree shape.

Acknowledgments

This study was partially funded by the Spanish Centre for the Development of Industrial Technology (CDTI) in the PROMETEO Project in the framework of the Consorcios Estratégicos Nacionales de Investigación Técnica (CENIT) program, the THERMOLIDAR FP7 Project and by AGL2012-40053-C03-01 (PJZT) from the Spanish "Ministerio de Economia y Competitividad. The authors are most grateful to the Treesat research group (ERSAF, University of Cordoba, Spain) for the support provided during the field campaigns.

Author Contributions

All authors made significant contributions to the manuscript. Rocío Hernández-Clemente was the main author who designed and performed the research, wrote the manuscript, interpreted and processed the data. Rafael Navarro-Cerrillo managed the project and contributed to the design of the research and reviewing the manuscript. Francisco Javier Romero-Ramírez pre-processed ALS data and participated in the field survey. Alberto Hornero pre-processed DAI data and participated in the design of the airborne data acquisition. Pablo Jesús Zarco-Tejada developed the methodology for the DAI data acquisition and processing and revised the manuscript.

Conflicts of Interest

The authors declare no conflict of interest.

References

1. Breunig, F.M.; Galvão, L.S; Formaggio, A.R.; Neves Epiphanio, J.C. Directional effects on NDVI and LAI retrievals from MODIS: A case study in Brazil with soybean. *Int. J. Appl. Earth Obs.* **2011**, *13*, 34–42.
2. Wang, Q.; Adiku, S.; Tenhunen, J.; Granier A. On the relationship of NDVI with leaf area index in a deciduous forest site. *Remote Sens. Environ.* **2005**, *94*, 244–255.
3. Birky, A.K. NDVI and a simple model of deciduous forest seasonal dynamics. *Ecol. Model.* **2001**, *143*, 43–58.
4. Maselli, F. Monitoring forest conditions in a protected mediterranean coastal area by the analysis of multiyear NDVI data. *Remote Sens. Environ.* **2004**, *89*, 423–433.
5. Heiskanen, J.; Rautiainen, M.; Stenberg, P.; Mõttus, M.; Vesanto, V.-H.; Korhonen, L.; Majasalmi, T. Seasonal variation in MODIS LAI for a boreal forest area in Finland. *Remote Sens. Environ.* **2012**, *126*, 104–115.
6. Busetto, L.; Michele M.; Colombo R. Combining medium and coarse spatial resolution satellite data to improve the estimation of sub-pixel NDVI time series. *Remote Sens. Environ.* **2008**, *112*, 118–131.

7. Tillack, A.; Clasen, A.; Kleinschmit, B.; Förster, M. Estimation of the seasonal leaf area index in an alluvial forest using high-resolution satellite-based vegetation indices. *Remote Sens. Environ.* **2014**, *141*, 52–63.
8. Darvishzadeh, R.; Atzberger, C.; Skidmore, A.; Schlerf, M. Mapping grassland leaf area index with airborne hyperspectral imagery: A comparison study of statistical approaches and inversion of radiative transfer models. *ISPRS J. Photogramm. Remote Sens.* **2011**, *66*, 894–906.
9. Morsdorf, F.; Kötz, B.; Meier, E.; Itten, K.I.; Allgöwer, B. Estimation of LAI and fractional cover from small footprint airborne laser scanning data based on gap fraction. *Remote Sens. Environ.* **2006**, *104*, 50–61.
10. Lee, A.C.; Lucas, R.M. A LiDAR-derived canopy density model for tree stem and crown mapping in Australian forests. *Remote Sens. Environ.* **2007**, *111*, 493–518.
11. Zhao, F.; Strahler, A.H.; Schaaf, C.L.; Yao, T.; Yang, X.; Wang, Z.; Schull, M.A.; Román, M.O.; Woodcock, C.E.; Olofsson, P.; *et al*. Measuring gap fraction, element clumping index and LAI in sierra forest stands using a full-waveform ground-based lidar. *Remote Sens. Environ.* **2012**, *125*, 73–79.
12. Solberg, S.; Næsset, E.; Hanssen, K.H.; Christiansen, E. Mapping defoliation during a severe insect attack on Scots pine using airborne laser scanning. *Remote Sens. Environ.* **2006**, *102*, 364–376.
13. Zhao, K.; Popescu, S. Lidar-based mapping of leaf area index and its use for validating GLOBCARBON satellite LAI product in a temperate forest of the southern USA. *Remote Sens. Environ.* **2009**, *113*, 1628–1645
14. Hall, S.A.; Burke, I.C.; Box, D.O.; Kaufmann, M.R.; Stoker, J.M. Estimating stand structure using discrete-return lidar: An example from low density, fire prone ponderosa pine forests. *For. Ecol. Manage.* **2005**, *208*, 189–209.
15. Næsset, E.; Bjerknes, K.-O. Estimating tree heights and number of stems in young forest stands using airborne laser scanner data. *Remote Sens. Environ.* **2001**, *78*, 328–340.
16. Treitz, P.; Lim, K.; Woods, M.; Pitt, D.; Nesbitt D.; Etheridge, D. LiDAR sampling intensity for forest resource inventories in Ontario, Canada. *Remote Sens.* **2012**, *4*, 830–848.
17. Næsset, E. Determination of mean tree height of forest stands by means of digital photogrammetry. *Scand. J. For. Res*. **2002**, *17*, 446–459.
18. Næsset, E. Predicting forest stand characteristics with airborne scanning laser using a practical two-stage procedure and field data. *Remote Sens. Environ.* **2002**, *80*, 88–99.
19. Holmgren, J.; Nilsson, M.; Olsson, H. Simulating the effects of LiDAR scanning angle for estimation of mean tree height and canopy closure. *Can. J. Remote Sens.* **2003**, *29*, 623–632.
20. González-ferreiro, E.; Diéguez-aranda, U.; Miranda, D. Estimation of stand variables in Pinus radiata D. Don plantations using different LiDAR pulse densities. *Forestry* **2012**, *85*, 281–292.
21. Magnusson, M.; Fransson, J.E.S.; Holmgren, J. Effects of estimation accuracy of forest variables using different pulse density of laser data. *For. Sci.* **2010**, *53*, 619–626.
22. Popescu, S.C.; Wynne, R.H. Seeing the trees in the forest: using LiDAR and multispectral data fusion with local filtering and variable window size for estimating tree height. *Photogramm. Eng. Remote Sens.* **2004**, *70*, 589–604.

23. Yu, X.; Hyyppä, J.; Kaartinen, H.; Maltamo, M. Automatic detection of harvested trees and determination of forest growth using airborne laser scanning. *Remote Sens. Environ.* **2004**, *90*, 451–462.
24. Popescu, S.C.; Wynne, R.H.; Nelson, R.H. Measuring individual tree crown diameter with LiDAR and assessing its influence on estimating forest volume and biomass. *Can. J. Remote Sens.* **2003**, *29*, 564–577.
25. Popescu, S.C.; Kaiguang, Z. A voxel-based LiDAR method for estimating crown base height for deciduous and pine trees. *Remote Sens. Environ.* **2008**, *112*, 767–781.
26. Hyyppä, J.; Inkinen, M. Detecting and estimating attributes for single trees using laser scanner. *Photogramm. J. Finl.* **1999**, *16*, 27–42.
27. Vauhkonen, J.; Tokola, T.; Packalén, P.; Maltamo, M. Identification of Scandinavian commercial species of individual trees from airborne laser scanning data using alpha shape metrics. *For. Sci.* **2009**, *55*, 37–47.
28. Järnstedt, J.; Pekkarinen, A.; Tuominen, S.; Ginzler, C.; Holopainen, M.; Viitala, R. Forest variable estimation using a high-resolution digital surface model. *ISPRS J. Photogramm. Remote Sens.* **2012**, *74*, 78–84.
29. Dandois, J.P.; Ellis, E.C. High spatial resolution three-dimensional mapping of vegetation spectral dynamics using computer vision. *Remote Sens. Environ.* **2013**, *136*, 259–276.
30. Berni, J.A.J.; Zarco-Tejada, P.J.; Suarez, L.; Fereres, E. Thermal and narrow-band multispectral remote sensing for vegetation monitoring from an unmanned aerial vehicle. *IEEE Trans. Geosci. Remote Sens.* **2009**, *47*, 722–738.
31. Haala, N.; Hastedt, H.; Wolf, K.; Ressl, C.; Baltrusch, S. Digital photogrammetric camera evaluation—Generation of digital elevation models. *Photogramm.-Fernerkund.-Geoinf.* **2010**, *2*, 98–15.
32. Baltsavias, E.; Gruen, A.; Eisenbeiss, H.; Zhang, L.; Waser, L.T. High quality image matching and automated generation of 3D tree models. *Int. J. Remote Sens.* **2008**, *29*, 1243–1259
33. St-Onge, B.; Hu, Y.; Véga, C. Mapping the height and above-ground biomass of a mixed forest using LiDAR and stereo Ikonos images. *Int. J. Remote Sen.* **2007**, *29*, 1277–1294.
34. Valbuena, R. Integrating airborne laser scanning with data from global navigation satellite systems and optical sensors. *Manag. For. Ecos*. **2014**, *27*, 63–88.
35. Zarco-Tejada, P.J.; Diaz-Varela, R.; Angileri, V.; Loudjani, P. Tree height quantification using very high resolution imagery acquired from an unmanned aerial vehicle (UAV) and automatic 3D photo reconstruction methods. *Eur. J. Agron.* **2014**, *55*, 89–99.
36. Moralejo, E.; García Muñoz, J.A.; Descals, E. Susceptibility of Iberian trees to Phytophthora ramorum and P. cinnamomi. *Plant pathol.* **2009**, *58*, 271–283.
37. Baatz, M.; Schäpe, A. Multiresolution segmentation: An optimization approach for high quality multi-scale image segmentation. In Proceedings of Angewandte Geographische Informationsverarbeitung XII. Beiträge zum AGIT-Symposium Salzburg 2000; Herbert Wichmann Verlag: Karlsruhe, Germany, 2000; pp. 12–23.
38. Axelsson, P. DEM generation from laser scanner data using adaptive TIN models. *Int. Arch. Photogramm. Remote Sens.* **2000**, *33*, 110–117.

39. McGauhey, R.J. *FUSION/LDV: Software for LiDAR Data Analysis and Visualization*; USDA Forest Service, Pacific Northwest Research Station: Seattle, WA, USA, 2009.
40. Curran, P.J.; Atkinson, P.M. Geostatistics and remote sensing. *Prog. Phys. Geogr.* **1998**, *22*, 61–78.
41. Freund, R.J.; Littell, R.C. *SAS System for Regression*; SAS Institute Inc.: Cary, NC, USA, 1986.
42. Belsley, D.A. A guide to using the collinearity diagnostics. *Comput. Sci. Econ. Manage.* **1991**, *4*, 33–50.
43. Korpela, I.; Anttila, P. Appraisal of the mean height of trees by means of image matching of digitised aerial photographs. *Photogramm. J. Finl.* **2004**, *19*, 23–36.
44. Bohlin, J.; Wallerman, J.; Fransson, J.E.S. Forest variable estimation using photogrammetric matching of digital aerial images in combination with a high-resolution DEM. *Scand. J. For. Res.* **2012**, *27*, 692–699.
45. Breidenbach, J.; Astrup, R. Small area estimation of forest attributes in the Norwegian National Forest Inventory. *Eur. J. For. Res.* **2012**, *131*, 1255–1267.
46. Persson, A.; Holmgren, J.; Söerman, U. Detecting and measuring individual trees using an airborne laser scanner. *Photogramm. Eng. Remote Sens.* **2002**, *68*, 925−932.
47. Feikema, P.M.; Morris, J.D.; Beverly, C.R.; Collopy, J.J.; Baker, T.G.; Lane, P.N.J. Validation of plantation transpiration in south-eastern Australia estimated using the 3PG+ forest growth model. *For. Ecol. Manage.* **2010**, *260*, 663–678.
48. Wang, Z.; Grant, R.F.; Arain, M.A.; Chen, B.N.; Coops, N.; Hember, R.; Kurz, W.A. Evaluating weather effects on interannual variation in net ecosystem productivity of a coastal temperate forest landscape: A model intercomparison. *Ecol. Model.* **2011**, *222*, 3236–3249.
49. Zhou, X.; Peng, C.; Dang, Q.L.; Chen, J.; Parton, S. Predicting forest growth and yield in northeastern Ontario using the process-based model of TRIPLEX1.0. *Can. J. For. Res.* **2005**, *35*, 2268–2280.